Inhibition of CO_2 corrosion of mild steel in a highly mineralized saline solution with a new synthesized α-aminophosphonate

Yu.P. Khodyrev,* E.N. Nikitin, G.G. Shumatbaev, K.O. Sinyshin, D.A. Terenzhev and A.M. Ermakova

A.E. Arbuzov Institute of Organic and Physical Chemistry, Subdivision of the Federal State Budgetary Institution of Science "Kazan Scientific Center of Russian Academy of Sciences", Arbuzov Str. 8, 420088 Kazan, Russian Federation
**E-mail: khyp@km.ru*

Abstract

The inhibitory effect of new synthesized neonylethyldiethylaminomethylphosphonate (NEDMP) on the CO_2 corrosion of mild steel was studied the methods of linear polarization resistance (LPR), potentiodynamic polarization and electrochemical impedance spectroscopy (EIS). The results show that NEDMP is a good inhibitor with an inhibition efficiency of 60–98% at concentrations of 0.5–25 ppm. The adsorption of inhibitor molecules on the surface of the steel submits the Langmuir adsorption isotherm. The corrosion rate grows with increasing temperature from 30 to 70°C; however, inhibitor efficiency decreased very slightly. NEDMP can be considered as a mixed type inhibitor with a predominant effect on the metal dissolution reaction. NEDMP molecules are desorbed from the metal surface with anodic polarization. The desorption potential relatively to the open circuit potential does not depend from the concentration of the inhibitor in the solution; it decreases linearly with increasing temperature. Kinetic and thermodynamic parameters were calculated. Analysis of these parameters showed that adsorption mechanism of the molecules of NEDMP on mild steel may involve two types of interaction: chemisorption and physisorption. The inhibitor molecules block the surface of the metal during spontaneous electrostatic adsorption. The part of the molecules that was adsorbed on the active centres of metal dissolution forms a coordination bond, possibly through an oxygen atom. An increase in temperature or potential accelerates this process.

Keywords: *steel, polarization, acid corrosion, inhibition.*

Received: April 9, 2019. Published: April 16, 2019 doi: 10.17675/2305-6894-2019-8-2-13

1. Introduction

Carbon dioxide corrosion is one of the major problems in the oil industry. Despite 40 years of intense research [1–7], the mechanism of the CO_2 corrosion of mild steel is still unclear, the reason is the high variability of aggressive media. Furthermore, corrosion products can change the corrosion rate, forming carbonate films on the surface of the steel [4, 5, 8–11]. Changes in temperature, pH values and the accumulation of Fe^{2+} ions in a solution change the concentration of CO_3^{2-}, HCO_3^-, H^+, OH^- and Cl^- ions in aggressive media [4, 5, 12–

16]. All these factors can affect both the mechanism of redox reactions on the surface of the steel, and chemical reactions in a liquid medium.

The use of inhibitors is the most effective and cheap way to protect steel from corrosion. Organic compounds, such as quaternary ammonium salts, amides, amines and imidazolines, have been used at concentration 10–100 ppm in the oil industry. Information about them is presented in detail in the reviews [17–19].

The diversity of the composition, acidity and temperature of the corrosive environment in various oil fields, as well as the requirements of environmental safety, indicate the need to expand the range of inhibitors of carbon dioxide corrosion of steel, effective at low concentrations over wide range temperatures. There is already some success in this direction. In fact, it was found that the inhibition efficiency reaches 80–98% in the concentration range of 0.2–5 ppm for mercaptopyrimidines [20], thiourea [21], ammonium salts of *O,O*-dialkyldithiophosphoric acid [22] and *N*-2-[(2-aminoethyl)-aminoethyl]-9-octadecenamide [23].

The overwhelming majority of studies on the inhibitory activity of organic compounds were carried out in low-mineralized medium with content of NaCl from 0.5 to 3 wt.%. Currently, in many fields, the concentration of NaCl can reach 25% by weight. Inhibitors that have proven themselves in a weakly mineralized environment can reduce inhibitory activity in highly mineralized multicomponent solutions. In this work, the inhibitory effect and the adsorption behaviour of a new synthesized neonylethyl-diethylaminomethylenephosphonate (NEDMP) were investigated during mild steel corrosion in a saturated CO_2 salt solution at a temperature of 30 to 70°C.

2. Experimental details

2.1. Synthesis of neonylethyldiethylaminomethylenephosphonate (NEDMP)

Synthesis of α-aminophosphonate was carried out according to the classical Kabachnik–Fields reaction, presented in Figure 1 [24].

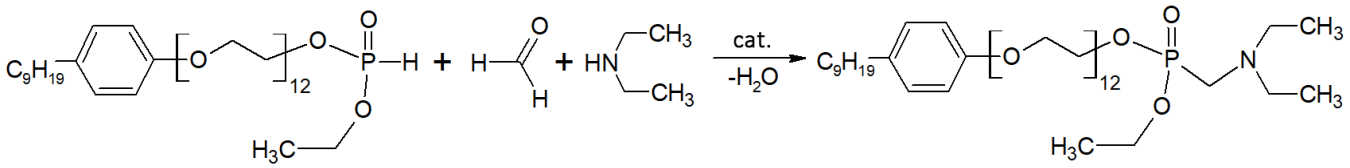

Figure 1. Scheme of neonylethyldiethylaminomethylenephosphonate synthesis.

15 ml of anhydrous benzene was added to the flask, then 2.5 g (0.003 mol) of *O*-(35-(4-Nonylphenoxy)-3,6,9,12,15,18,21,24,27,30,33-undecaoxapentatriacontanyl-1-)-*O*-ethyl phosphite, 0.3 g (0.004 mol) of diethylamine, 0.1 g of paraform (0.003 mol in terms of formaldehyde), and 0.01 g of *p*-toluene sulfonic acid as the catalyst were successively added with stirring. The mixture was stirred at 60°C for 20 hours under argon stream. After completion of the reaction the catalyst was removed. 1 g of sodium carbonate was poured

into the flask, which was stirred for 1 hour at 60°C and filtered; the filtrate was washed with 5 ml of benzene. The filtrate was then evaporated for 1 hour in a vacuum (0.02 mmHg) at 60°C. The weight of end product was 1.2 g. The yield of *O*-(35-(4-nonylphenoxy)-3,6,9,12,15,18,21,24,27,30,33-undecaoxapentatriacontanyl-1-)-*O*-ethyl-(-(*N*,*N*-dimethyl)aminomethylene)phosphonate was 40%. The obtained precipitate was recrystallized from ethanol. The chemical structure of the synthesized inhibitor is shown in Figure 1. The structure and purity of the compound were confirmed by FT-IR and ^{1}H, ^{13}C, ^{31}P NMR spectroscopic methods.

IR spectrum, ν cm^{-1}: 1250 (P=O); ^{1}H NMR spectrum ($CDCl_3$), δ ppm: 0.72 t (3H, $C\underline{H}_3CH_2CH_2$, $^{3}J_{HH}$ = 7.0); 0.77 t [6H, $(C\underline{H}_3CH_2)_2N$, $^{3}J_{HH}$ = 5.5]; 1.00–1.24 m (CH_2); 1.35 t (3H, $C\underline{H}_3CH_2OP$, $^{3}J_{HH}$ = 7.0); 1.44–1.65 m (CH_2); 2.92 q [4H, $(CH_3C\underline{H}_2)_2N$, $^{3}J_{HH}$ = 7.0]; 3.04 m (CH_2); 3.12 d (2H, PCH_2N, $^{2}J_{PH}$ = 13.2); 3.25 t (2H, $CH_2C\underline{H}_2Ar$, $^{3}J_{HH}$ = 7.2); 3.62–3.67 m (OCH_2CH_2O); 3.80 t (2H, $POCH_2C\underline{H}_2O$, $^{3}J_{HH}$ 4.7); 3.95 m (2H, $POC\underline{H}_2CH_2O$); 4.07 t (2H, $ArOC\underline{H}_2CH_2O$, $^{3}J_{HH}$ 4.7); 4.18 m (2H, $POC\underline{H}_2CH_3$); 6.78 d (2H, CH Ar, $^{3}J_{HH}$ = 8.5); 7.24 d (2H, CH Ar, $^{3}J_{HH}$ = 8.9). ^{13}C NMR spectrum, δ_C ppm (*J*, Hz) (the data given in parentheses are for the ^{13}C–{^{1}H} spectra): 10.96 q (s) [$\underline{C}H_3CH_2N$-, $^{1}J_{CH}$ =128]; 11.58 q (s) [$\underline{C}H_3CH_2CH_2$–, $^{1}J_{CH}$ = 128]; 13.93 q (s) [$\underline{C}H_3CH_2O$–, $^{1}J_{CH}$ = 124.1]; 23.86 t (s) [$CH_3\underline{C}H_2CH_2$–, $^{1}J_{CH}$ = 122.9]; 29.79 t (s) [$CH_3CH_2\underline{C}H_2$–, $^{1}J_{CH}$ = 143.05]; 32.45 t (s) [–$CH_2CH_2CH_2$–, $^{1}J_{CH}$ = 122.5]; 41.65 t (s) [–$\underline{C}H_2$–Ar, $^{1}J_{CH}$ = 142.3]; 43.61 t (s) [$CH_3\underline{C}H_2N$–, $^{1}J_{CH}$ = 104.09]; 49.1 m (d) [–$\underline{C}H_2$–P–, $^{1}J_{CP}$ = 123.2]; 61.3 t (s) [$CH_3\underline{C}H_2O$–, $^{1}J_{CH}$ = 139.2]; 67.09 t (s) [–$OCH_2\underline{C}H_2O$–P, $^{1}J_{CH}$ = 141.9]; 67.16 t (s) [–$O\underline{C}H_2CH_2O$–, $^{1}J_{CH}$ = 141.9]; 69.63 t (s) [–$O\underline{C}H_2\underline{C}H_2O$–, $^{1}J_{CH}$ = 141.6]; 70.17 t (s) [–$O\underline{C}H_2\underline{C}H_2O$–, $^{1}J_{CH}$ = 141.6]; 70.26 t (s) [–$O\underline{C}H_2\underline{C}H_2O$–, $^{1}J_{CH}$ = 141.6]; 70.39 t (s) [$(-O-\underline{C}H_2\underline{C}H_2-O-)_n$, $^{1}J_{CH}$ = 140.9]; 70.60 t (s) [–O–$\underline{C}H_2\underline{C}H_2O$–, $^{1}J_{CH}$ = 140.9]; 72.51 t (s) [–$O\underline{C}H_2\underline{C}H_2O$–, $^{1}J_{CH}$ = 140.5]; 113.6 d (s) [–CH_2–C_{ar}–$\underline{C}H_{ar}$, $^{1}J_{CH}$ = 158.9]; 127.42 d (s) [–O–C_{ar}–$\underline{C}H_{ar}$, $^{1}J_{CH}$ = 154.8]; 139.65 s (s) [–CH_2–$\underline{C}_{ar}$]; 156.06 s (s) [–O–$\underline{C}_{ar}$]. ^{31}P–{^{1}H} NMR spectrum ($CDCl_3$): δ_P 26.1 ppm. Found, %: C 60.23; H 9.52; N 1.71; P 3.78. $C_{46}H_{88}NO_{15}P$. Calculated, %: C 60.51; H 9.65; N 1.76; P 3.90.

2.2. Material preparation

The aggressive solution (NaCl – 163, $CaCl_2 \cdot 2H_2O$ – 23, $MgCl_2 \cdot 6H_2O$ – 17, $CaSO_4 \cdot 2H_2O$ – 1.4 g L^{-1}) was prepared by dissolving of analytical amounts in distilled water. CO_2 was bubbled through the solution in a 1 L electrochemical cell. The electrodes were immersed in the cell after reaching the equilibrium distribution of ions and hydrated particles formed during the dissolution of CO_2 in brine. The equilibrium was controlled by the stability of the pH value, which was 5.3 for a saturated solution. The experiments were carried out at 30–70°C with a temperature control of ±1°C. During the experiments, a small gas pressure was maintained in the chamber to protect it from air pollution. The solution was magnetically stirred at a speed of 500 rpm. Electrochemical measurements were performed with three similar working electrodes from 1018 MS of 30.7 mm length and 4.7 mm diameter used in turn during subsequent experiments. Before each experiment, electrodes

were treated with abrasive paper (1200 grit SiC), etched with 10% HCl solution for 10 min, washed with distilled water, then acetone, dried by warm air and then immediately placed into the cell.

2.3. Electrochemical measurements

Electrochemical measurements were carried in a three-electrode cell with a Ag/AgCl/KCl saturated reference electrode (SSE) and platinum mesh as the counter electrode. Polarization and impedance measurements were performed using a Field Machine potentiostat (ICM Instrument). Linear polarization resistance measurements were conducted at 0.5 h intervals in the potential range of ±5 mV with respect to the open circuit potential (OCP) at a scan rate of 0.5 mV s^{-1}. The polarization resistance values obtained (R_p) were transferred into corrosion rates I_{cor} [25] using Eq. (1):

$$I_{cor} = \frac{b_a b_c}{2.3(b_a + b_c)R_p} \quad (1)$$

where b_a and b_c are Tafel coefficients obtained from potentiodynamic curves.

Inhibition efficiency (*IE*) and surface coverage (θ) were calculated using the following Equations (2, 3):

$$IE(\%) = 100 \cdot (I_0 - I_i) / I_0 \quad (2)$$

$$\theta = (I_0 - I_i) / I_0 \quad (3)$$

where I_0 and I_i are corrosion rates in the brine without and with inhibitor, respectively.

Impedance measurements were performed at OCP over the frequency region 10 MHz–30 kHz by applying AC signal with 5 mV amplitude. Polarization measurements were performed at the end of experiment in a range from +30 to –120 mV (0.5 cycles) for cathode and from –30 to +250 mV (1 cycle) *vs*. OCP for anode regions with the scan rate of 1 mV s^{-1}. Preliminary experiments have shown that polarization in any direction relative to the corrosion potential leads to irreversible changes in the metallic surface. This was the reason for using three identical work electrodes during the experiment. One of the three electrodes was used for LPR and EIS measurements, and two electrodes, which were in brine at the open circuit potential, were used in series for cathodic and anodic polarization.

3. Results and discussion

3.1. LPR measurements

Polarization and impedance measurements require the stability of the system under study during long-term experiments. Figure 2 shows the changes in polarization resistance as a function of time after the working electrode is immersed in a solution with different concentrations of NEDMP at 40°C. The growth of the values of R_p began almost immediately and the stable value of the corrosion potential (E_{corr}) was established 2 hours

after the immersion. As can be seen in Figure 2, the time to reach stationary R_p values increased with an increase in the concentration of NEDMP and reached 10 hours for the maximum concentration. This determined the start time of the impedance and polarization measurement since the change current can lead to distorted results.

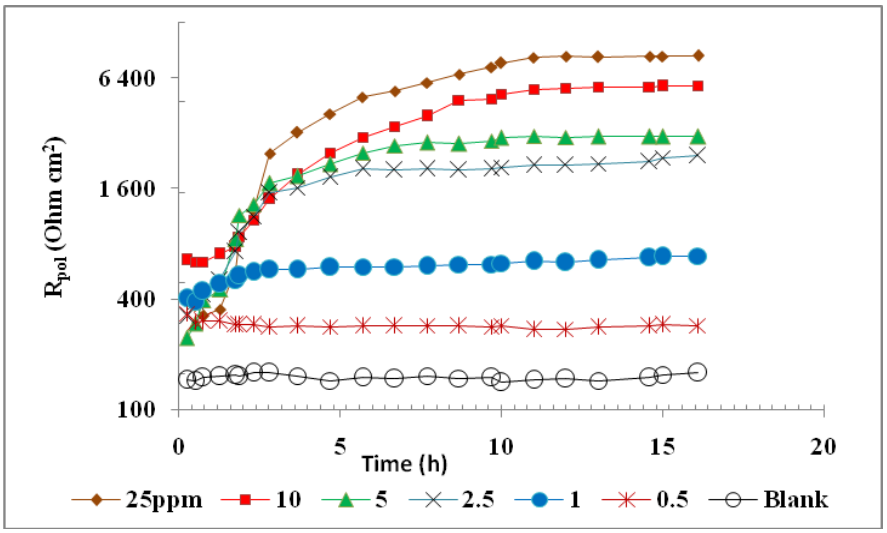

Figure 2. Variations of the polarization resistance on time for mild steel in CO_2- saturated test brine with different concentration of NEDMP at 40°C.

3.2. Potentiodynamic measurements

Figure 3 shows cathodic and anodic polarization plots of mild steel in CO_2 saturated solution with different concentrations of NEDMP at 40°C. The polarization curve in the Blank solution is different from the curve obtained earlier using an aggressive medium containing 3% NaCl [20, 22]. The corrosion potential shifted in the positive direction by 20 mV. The values of b_c, b_a and I_{cor} were previously –444, 62 mV/dec and 197 μA/cm^{-2}, and now 63, 313 mV/dec and 145 μA cm^{-2}, respectively. A similar polarization curve for the Blank was obtained for a highly mineralized medium with a concentration of 90.44 g/L NaCl [26] and with 3 M NaCl [16]. The decrease in I_{cor} with an increase in NaCl concentration from 3 to 16.3% may be due to a drop in the solubility of carbon dioxide and a decrease in the mobility of electroactive anions. An increase in the inhibitor concentration in the test solution leads to a consistent decrease in both anodic and cathodic current densities and a shift the corrosion potential towards positive values.

In a number of works [26], it was proposed to characterize inhibitors with a shift in the corrosion potential relative to the Blanck potential. With a shift greater than 85 mV, the inhibitor is considered as an anodic or cathodic inhibitor. NEDMP can be considered as a mixed-type inhibitor with a predominant effect on the anodic process, since the shift of the corrosion potential to positive values does not exceed 70 mV and a significant more drop in anodic currents is observed compared to cathodic currents.

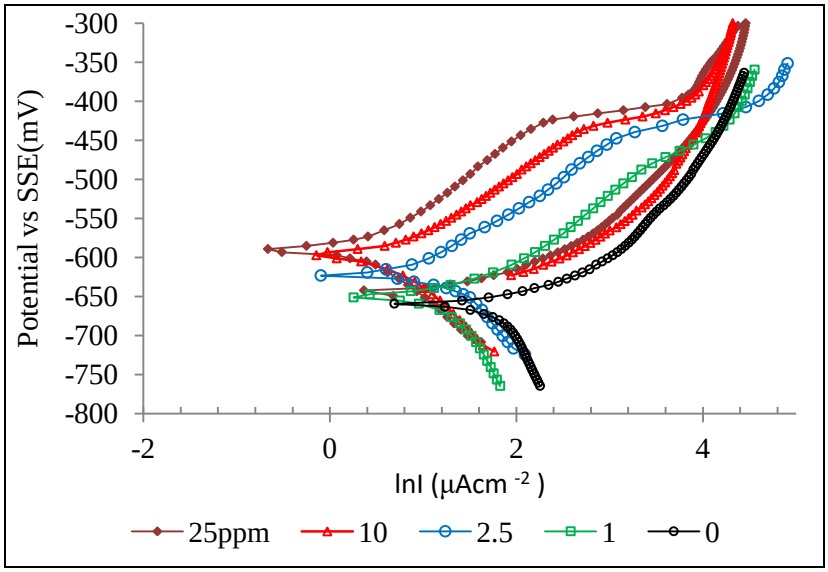

Figure 3. Polarization curves of mild steel obtained at 40°C in CO_2 saturated brine with different concentrations of NEDMP.

Table 1 demonstrates the electrochemical parameters, such as the corrosion potential (E_{corr}), difference of potentials (E_{des}–E_{cor}), cathodic and anodic Tafel slopes (b_c and b_a), corrosion current densities and inhibition efficiencies (I_{cor}^{extr} and IE_{cor}^{extr}) determinated by extrapolation of Tafel lines as well as R_p, I_{cor}^{LPR} and IE_{cor}^{LPR} values obtained from LPR measurements using equations (1–3).

Table 1. Electrochemical parameters obtained from polarization curves and LPR methods in a CO_2-saturated test solution with different concentrations of NDPM at different temperatures.

T (°C)	C (ppm)	E_{cor} (mV)	E_{des}–E_{cor} (mV)	b_a mV/dec	$-b_c$ mV/dec	I_{cor}^{extr} μA cm^{-2}	IE_{cor}^{extr} (%)	LPR Ohm cm^2	I_{cor}^{LPR} μA cm^{-2}	IE_{cor}^{LPR} (%)
40	25	–588	160	60	80	1.8	98.8	8470	1.76	98.9
40	10	–595	155	82	160	3.5	97.5	6780	4.06	97.2
40	5	–616	164	78	180	6.0	95.8	3131	7.7	94.6
40	2.5	–615	167	83	210	8.9	92.8	2416	10.7	92.5
40	1	–617	164	70	220	29.8	79.4	690	33.5	76.8
40	0.5	–647	–	45	259	53.0	57.5	289	57.7	60.1
30	0	–659	–	63	349	120	–	198	130	–
40	0	–660	–	63	313	144	–	160	145	–
50	0	–665	–	60	270	175	–	117	182	–
60	0	–660	–	60	255	210	–	96	220	–
70	0	–668	–	56	240	251	–	75	233	–

T (°C)	C (ppm)	E_{cor} (mV)	$E_{des}-E_{cor}$ (mV)	b_a mV/dec	$-b_c$ mV/dec	I_{cor}^{extr} μA cm^{-2}	IE_{cor}^{extr} (%)	LPR Ohm cm^2	I_{cor}^{LPR} μA cm^{-2}	IE_{cor}^{LPR} (%)
30	25	–585	185	50	90	1.6	98.7	10650	1.22	98.9
50	25	–604	133	41	80	5.8	96.7	2750	4.29	97.6
60	25	–619	118	45	100	10.6	95.0	1689	7.99	96.4
70	25	–614	93	48	90	15.6	93.2	1023	13.3	94.3

With anodic polarization, the curves in solution with the inhibitor changed dramatically with respect to the curve for a solution without an inhibitor due to a significant decrease in current density and the appearance of a second linear region, where the currents sharply increased to values characteristic of a curve in solution without an inhibitor. The reverse scan curve for a solution with NEDMP is approaching the curve for a solution without an inhibitor. This indicates that the intersection potential of two linear sections can be defined as the potential for desorption of inhibitor molecules from the steel surface. Such behaviour was reported when studying carbon dioxide corrosion of iron in inhibited solutions with some organic compounds, for example, with thiourea [21], amphiphilic amidoamine [23], 2-mercaptopyrimidines [20, 22] and imidazolines [16, 26]. As shown in Table 1, $E_{des}-E_{cor}$ is practically constant for all concentrations of inhibitor. The desorption regions during cathode polarization were not observed. Extrapolation of Tafel lines and LPR measurements give similar inhibition efficiencies.

3.3. Electrochemical impedance studies

Figures 4(b) and (c) show Nyquist plots for mild steel in a saturated CO_2 test solution with different NEDMP content at 40°C. The Nyquist plot, usually observed in saturated CO_2 brine [20, 27], consists of a large capacitive semicircle and inductive loops at a lower frequency. A semicircle is associated with a charge transfer process, and an inductive loop can be associated with the dissolution of a metal through the formation of an intermediate reaction product on the surface [27, 28]. As can be seen from Figure 4, the diameter of the semicircles increases and the inductive loop disappears with increasing concentration of the synthesized NEDMP in solution. If the semicircle has a centre below the axis, the ideal capacitance is often replaced by a constant phase element (CPE).

The behavior of the electrochemical system under study was simulated using the equivalent circuit shown in Figure 4(a), where R_{ct} and R_s is charge transfer resistance and resistance of solution, respectively. The impedance Z_{CPE} is described as follows [29]:

$$Z_{CPE} = Q^{-1}(j\omega)^{-n} \quad (4)$$

where Q is CPE constant, ω the angular frequency, $j=\sqrt{-1}$ and n is the phase shift.

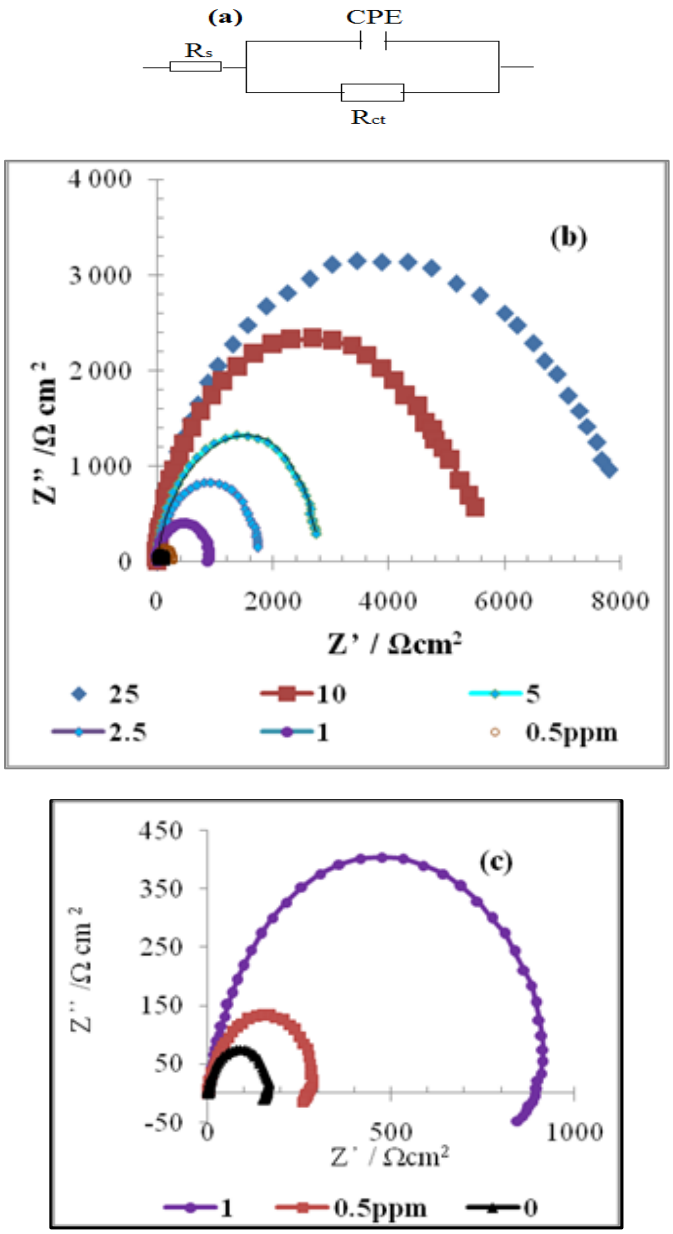

Figure 4. Equivalent circuit and Nyquist plots for mild steel in CO_2 saturated test solution with various concentrations of NEDMP at 40°C.

Various parameters such as R_{ct}, C_{dl}, n, were determined using MEISP software and listed in Table 2, where the *IE*% values were calculated using Eq. (1) where R_p was replaced with R_{ct}. With a growth in the NEDMP concentration, R_{ct} values increase and C_{dl} values decrease due to the formation of an adsorbed film of inhibitor molecules on the metal surface.

Table 2. Electrochemical parameters of impedance and the inhibition efficiencies for mild steel in CO_2 saturated test solution at different temperatures with various concentrations of NEDMP.

T (°C)	C (ppm)	R_s (Ω cm^2)	R_{ct} (Ω cm^2)	C_{dl} (μF cm^{-2})	n	IE (%)
40	25	2.3	7786	167	0.907	98.6
40	10	2.2	5299	212	0.903	96.8
40	5	7.6	2927	195	0.916	94.1
40	2.5	1.9	1789	261	0.888	89.5
40	1	3.1	963	383	0.872	82.6
40	0.5	3.0	293	930	0.918	58.7
30	0	2.2	231	1012	0.870	–
40	0	2.3	165	1340	0.928	–
50	0	2.1	122	1333	0.886	–
60	0	2.3	108	1080	0.893	–
70	0	2.2	86	740	0.891	–
30	25	1.2	9828	77	0.892	98.6
50	25	2.6	2707	180	0.902	97.5
60	25	2.5	2460	209	0.907	97.1
70	25	1.7	1590	221	0.923	96.3

3.4. Effect of temperature

Temperature has a great effect on the rate of metal electrochemical corrosion. Temperature dependence of the inhibitor efficiency and the comparison of the values of activation energy (E_a) of the corrosion process both in the absence and in the presence of inhibitors lead to some conclusions concerning the inhibition mechanism. An increase in temperature from 30 to 70°C gives a sharp decrease in the solubility of carbon dioxide in water, which leads to a decrease in the concentration of charged particles of CO_3^{2-}, HCO_3^-. The effect of temperature on the corrosion rates and polarization curves is shown in Table 1 and Figure 5, respectively. The corresponding electrochemical parameters of mild steel corrosion in brine at different temperatures in the absence and presence of 25 ppm NEDMP and calculated values are listed in Table 1. From Figure 5 and Table 1 it can be seen that the corrosion potential shifts to the negative region and the corrosion rates increase with temperature for both the anodic and cathodic reactions with and without the inhibitor. The inhibition efficiencies calculated from impedance results showed a similar tendency to those obtained from polarization measurements.

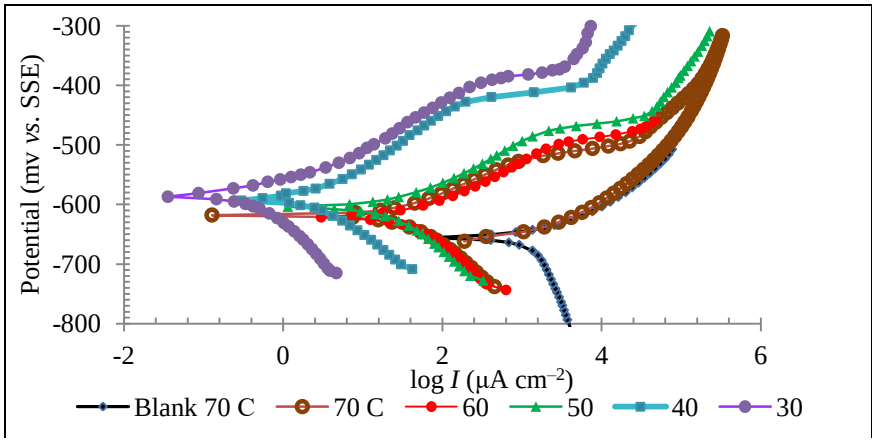

Figure 5. Polarization curves for mild steel obtained at different temperatures in CO_2 saturated test solution containing 25 ppm of NEDMP.

As it can be see from Table 2 and Figure 6, the values of R_{ct} decrease and those of C_{dl} increase with temperature. That may be interpreted as physical adsorption of NEDMP molecules to the metal surface with the adsorption–desorption equilibrium shifted towards desorption with growth of temperature.

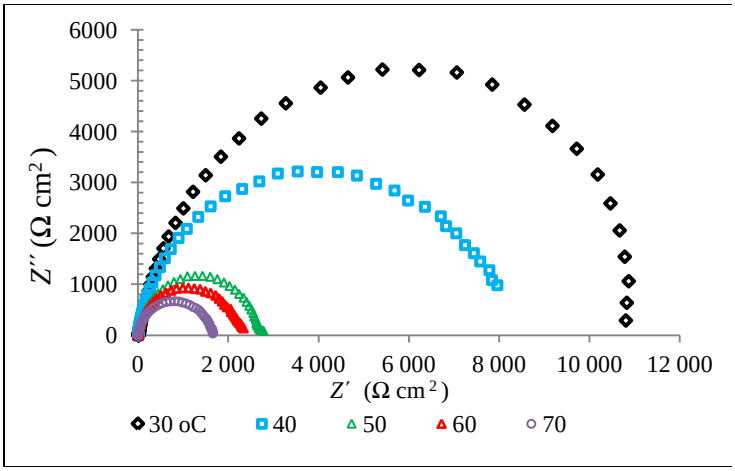

Figure 6. Nyquist graphs for mild steel at various temperatures in a CO_2-saturated test solution with 25 ppm NEDMP.

The inhibition efficiency remains high and almost constant with the increase of temperature suggesting that chemical adsorption mainly occurs. The weak dependence of IE on temperature indicates that the inhibitor is efficient in studied temperature region (30–70°C). As one would expect, the potential of desorption decreased with growth of temperature. It should be noted, that the slope and length of the second linear section of the anodic polarization curve remain almost unchanged with increasing temperature. Perhaps this is because most of the inhibitor molecules are firmly bound to the metal surface.

The relationship between the rate of corrosion of metal in aggressive media and temperature can be expressed by the Arrhenius equation:

$$I = A\exp\left(-E_a/RT\right) \quad (4)$$

where A is a constant and E_a is the apparent activation energy of the metal dissolution reaction.

Figure 7 shows Arrhenius plots of the logarithm of the current density vs $1/T$ for mild steel in the corrosive medium with absence and presence 25 ppm of NEDMP. The E_a values were determined from the slope of straight lines ($-E_a/R$) and are given in Table 3. The calculated value of E_a in the presence of an inhibitor is more than 4 times greater than E_a in a solution without an inhibitor. Many studies [27, 28] showed that in the presence of inhibitor the increase in E_a with respect to uninhibited solution could be interpreted as physical adsorption. A large difference E_a (NEDMP)–E_a (Blank) indicates a high inhibition of the dissolution of the metal. Tan *et al*. [30] showed the heterogeneity of the energetic surface using the wire beam electrodes method and found that the potential difference between active centers of the surface at CO_2 corrosion of mild steel was about 29 mV. The NEDMP molecules are adsorbed primarily on the most active centres where the corrosion rate significantly exceeds the average rate, which leads to an increase in the activation energy. This is also indicated by the high value of inhibitory activity at very low concentrations of NEDMP in Table 1.

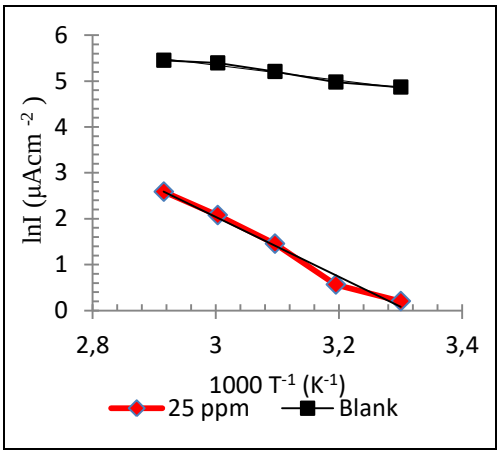

Figure 7. Arrhenius plots ln I_{corr} *vs*. $1/T$ for mild steel in CO_2 saturated test solution containing 25 ppm of NEDMP.

$$I_{cor} = \frac{RT}{N\hbar}\exp\left(-\frac{\Delta H_a^0}{RT}\right)\exp\left(\frac{\Delta S_a^0}{R}\right) \quad (5)$$

where N is Avogadro constant, $\hbar$ is Planck constant, ΔH_a^0 and ΔS_a^0 are the enthalpy and the entropy of activation, respectively.

Figure 8 shows that the plot of ln(1/*T*) *vs*. 1000/*T* is a straight line. The values of ΔH_a^0 and ΔS_a^0 can be calculated from the slope ($\Delta H_a^0 / R$) and intercept [ln(*R*/*Nħ*)+($\Delta S_a^0 / R$)]. Corrosion activation parameters are presented in Table 3.

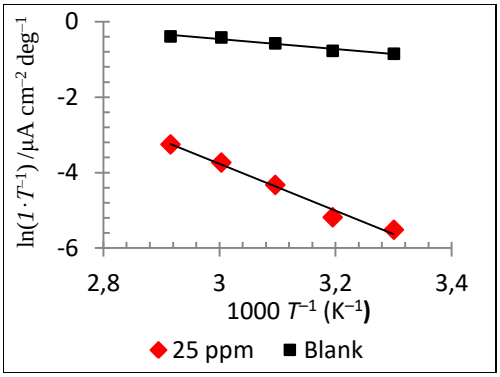

Figure 8. Arrhenius plots ln(1/*T*) vs. 1000/*T* for mild steel in CO_2 saturated test solution with 25 ppm of NEDMP.

Table 3. Thermodynamic parameters obtained from Arrhenius plots for mild steel in CO_2 saturated test solution.

	ΔG_{ads}^0 kJ mol^{-1}	ΔH_{ads}^0 kJ mol^{-1}	ΔS_{ads}^0 J mol^{-1} K^{-1}	E_a kJ mol^{-1}	ΔH_a^0 kJ mol^{-1}	ΔS_a^0 J mol^{-1} K^{-1}
NEDMP	–39.0	–42.0	–9.5	54.2	51.6	–8.4
Blank				13.7	11.1	–19.3
R^2 (NEDMP)	0.9946	0.9832		0.985	0.983	
R^2 (Blank))				0.973	0.959	

3.5. Adsorption isotherm

Adsorption isotherms describe the relationship between the molecular content in solution and the degree of surface coverage. The most commonly used isotherms (Langmuir, Temkin, Frumkin, and Freundlich) were used to identify the association with the concentration of NEDMP in solution. Table 4 shows the results of fitting the experimental data with different isotherms along with the adsorption coefficient (Bads). R^2 and *C* in Table 4 are the correlation coefficient and inhibitor concentration in brine, respectively, n is a constant value. Correlation coefficients indicate that the Langmuir isotherm presented in Figure 9 provides a better description of the experimental data using LPR data. The Bads value was determined from the slope of a straight line on the Langmuir adsorption graph. A high B_{ads} value indicates a strong adsorption ability of NEDMP molecules.

Table 4. The results of fitting experimental data with different isotherms.

Isotherm	Equation	R^2	B_{ads}
Langmuir	$\theta/(1-\theta) = B_{ads}C$	0.995	3251000
Frumkin	$\theta/(1-\theta) = B_{ads}Ce^{2a\theta}$	0.83	
Temkin	$\theta = B_{ads} \ln C$	0.70	
Freundlich	$\theta = B_{ads}C^n$	0.58	

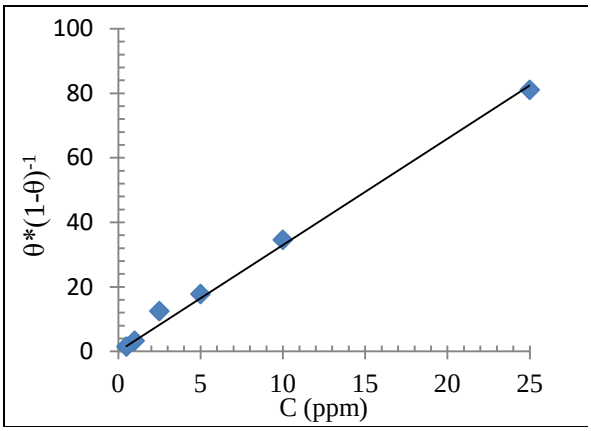

Figure 9. Langmuir adsorption plot for mild steel in CO_2 saturated test solution at 40°C.

The coefficient of adsorption of B_{ads} is connected with the standard free energy of adsorption (Goads) by the equation:

$$B_{ads} = \exp\left(-\frac{\Delta G^0_{ads}}{RT}\right) \quad (6)$$

The value ΔG^0_{ads} was determined from the slope of a straight line in the $\ln(\theta\cdot(1-\theta)^{-1})$ plots depending on T^{-1} (Figure 10) and is given in Table 4. It is known that the values of ΔG^0_{ads} below –20 kJ/mol are consistent with physical adsorption [31, 32], whereas values around –40 kJ/mol or higher are the result of separation or transfer of charge into the metal to form a coordinate bond. The obtained ΔG^0_{ads} value (–39.06 kJ mol^{-1}) indicates that the NEDMP adsorption mechanism on mild steel may include two types of interaction: chemisorption and physisorption.

The standard enthalpy ΔH^0_{ads} was determined in accordance with the Van't Hoff equation (Equation 7) by the slope of the straight line on the graphs $(-\Delta H^0_{ads}R^{-1})$ depending on T^{-1} (Figure 10) and is given in Table 3.

$$\ln B_{ads} = -\frac{\Delta H^0_{ads}}{RT} + Const \quad (7)$$

The value of ΔH^0_{ads} for physisorption is –40 kJ mol^{-1}, while for chemisorption it is –100 kJ mol^{-1} [33]. The calculated in this study the high negative value of ΔH^0_{ads} indicates that adsorption of NEDMP molecules on metal surface is exothermal process, which may involve complex interaction: mixture of the physisorption and chemisorption.

The standard entropy of adsorption ΔS^0_{ads} was calculated according to thermodynamic basic equation

$$\Delta G^0_{ads} = \Delta H^0_{ads} - T\Delta S^0_{ads} \quad (8)$$

The values of adsorption parameters derived from Arrhenius plots are listed in Table 3.

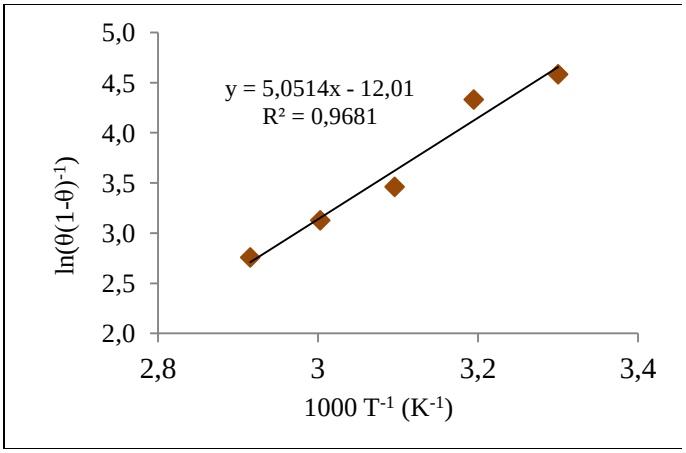

Figure 10. Dependence of $\ln(\theta\cdot(1-\theta)^{-1})$ *vs.* T^{-1} for mild steel in brine containing 25 ppm NEDMP.

The combination of activation and adsorption parameters obtained from Arrhenius plots indicate that the adsorption of the molecules of NEDMP on the steel surface can be carried out simultaneously as physisorption and chemisorption. The inhibitor molecules are adsorbed primarily on the most active centers, where the corrosion rate significantly exceeds the average rate, which leads to an increase in the activation energy. This is also indicated by the high value of inhibitory activity at very low concentrations of the molecules of NEDMP, which are shown in Table 1. It can be suggested, that the physisorption is the first stage of the corrosion inhibition, as a result of which molecules of the inhibitor replaces some of the molecules – H_2O, CO_2 and/or CO_3^{2-}, HCO_3^-, OH^- ions adsorbed on the metal surface [33]. In the second, slower stage, a part of the molecules that are adsorbed on the active centers of metal dissolution, form a coordination bond with the positive active center, possibly through an oxygen atom. An increase in temperature or potential should accelerate this process. However, the Langmuir isotherm implies that NEDMP molecules are adsorbed as a monolayer on a homogeneous surface and don't interact with each other, even when the metal surface is completely filled. This

contradiction is eliminated if assume that two disordered interdependent systems are formed on the metal surface, one of which follows the kinetic laws (physisorption), other is strongly bound Fe–NEDMP complexes (chemisorptions). The presence of such systems explains the desorption of NEDMP molecules, due to anodic polarization with transfer of the electron from molecule to the metal, to achieve a stable state for the Fe–brine–inhibitor system for a long time.

Conclusion

NEDMP was synthesized and characterized by spectral methods – IR spectroscopy, {^{1}H}-NMR and {^{13}C}-NMR spectroscopy. The results showed that NEDMP is a good inhibitor of carbon dioxide corrosion of mild steel in a highly mineralized saline solution with an inhibition efficiency of 60–98% at concentrations of 0.5–25 ppm. The inhibition efficiency increased with an increase in the inhibitor content in the solution and decreased slightly with an increase in temperature. Polarization studies showed that NEDMP can be attributed to mixed-type inhibitors with a more significant effect on the anodic process. NEDMP molecules were desorbed from the surface of the steel at high anodic potential, which decreases with increased of temperature. This indicates a strong bond between the EDMP molecules and the surface of the steel. The adsorption of NEDMP molecules on the surface of the steel is consistent with the Langmuir isotherm. The combination of the calculated thermodynamic parameters indicates that the adsorption of NEDMP molecules on the steel surface can be carried out simultaneously through physisorption and chemisorption.

Acknowledgements

The authors would like to thank Federal Research Center “Kazan Scientific Center of the Russian Academy of Sciences” for the research.

Funding

The authors are grateful for the financial support of the Russian Science Foundation, project No. 17-73-10273, title: “Synthesis and study of the mechanism of action of new active inhibitors of carbon dioxide and hydrogen sulfide corrosion of steels and non-ferrous metals for use in the oil industry”.

References

1. C. de Waard, U. Lotz and D.E. Milliams, *Corrosion,* 1991, **47**, 976. doi: 10.5006/1.3585212
2. B.R. Linter and G.T. Burstein, *Corros. Sci*., 1999, **41**, 117. doi: 10.1016/S0010-938X(98)00104-8
3. S. Nesic, *Corros. Sci*., 2007, **49**, 4308. doi: 10.1016/j.corsci.2007.06.006

4. L.G.S. Gray, M.J.D. Anderson, M.J. Danysh and B.G. Tremaine, *Corrosion/89*, 1989, paper no. 464.
5. L.G.S. Gray, M.J.D. Anderson, M.J. Danysh and B.G. Tremaine, *Corrosion/90*, 1990, paper no. 40.
6. G. Schmitt and S.Feinen, *Corrosion 2000*, 2000, paper no. 1.
7. F.M. Song, *Electrochim. Acta*, 2010, **55**, 689. doi: 10.1016/j.corsci.2017.10.005
8. B. Ingham, M. Kob, G. Kear, P. Kappen, N. Laycock, J.A. Kimpton and D.E. Williams, *Corros. Sci*., 2010, **52**, 3052. doi: 10.1016/j.corsci.2010.05.025
9. J. Han, S. Nesic, Y. Yang and B.N. Brown, *Electrochim. Acta*, 2011, **56**, 5396. doi: 10.1016/j.electacta.2011.03.053
10. J.L. Mora-Mendoza and S. Turgoose, *Corros. Sci*., 2002, 44, 1223. doi: 10.1016/S0010-938X(01)00141-X
11. E.W.J. Van Hunnik, B.F.M. Pots and E.L.J.A. Hendriksen, *Corrosion/96*, 1996, paper no. 6.
12. X. Jiang, Y.G. Zheng and W. Ke, *Corros. Sci*., 2006, **48**, no. 10, 309. doi: 10.1016/j.corsci.2005.12.002
13. Z. Lu, Y. Qiu and X. Guo, *Acta Phys., Chim. Sin*., 2008, **24**, no. 2, 243–249.
14. L.S. Moiseeva and N.S. Rashevskaya, *Russ. J. Appl. Chem.*, 2002, **75**, 1625 (in Russian). doi: 10.1023/A:1022223617203
15. K. Videm, *Corrosion/93*, 1993, paper no. 83.
16. X. Zhang, F. Wang, Y. He and Y. Du, *Corros. Sci*., 2001, **43**, 417. doi: 10.1016/S0010-938X(00)00160-8
17. E.S. Ivanov, *Inhibitors of Metal Corrosion in Acid Media*, *Metallurgiya*, Moscow, 1986 (in Russian).
18. B.J. Usman and S.A. Ali, *Arab. J. Sci. Eng*., 2017, **43**, 1. doi: 10.1007/s13369-017-2949-5
19. M. Finšgar and J. Jackson, *Corros. Sci*., 2014, **86**, 17. doi: 10.1016/j.corsci.2014.04.044
20. V.S. Reznik, V.D. Akamsin, Yu.P. Khodyrev, R.M. Galiakberov, Yu.Ya. Efremov and L. Tiwari, *Corros. Sci*., 2008, **50**, 392. doi: 10.1016/j.corsci.2007.06.021
21. X.Y. He, H.Y. Deng, R. Li, X.D. Fei, H.Y. Wang and Z.Y. Deng, *Acta Metall. Sin. (Engl. Lett.)*, 2008, **21**, no. 1, 65. doi: 10.1016/S1006-7191(08)60021-6
22. Yu.P. Khodyrev, E.S. Batyeva, E.K. Badeeva, E.V. Platova, L. Tiwari and O.G. Sinyashin, *Corros. Sci*., 2011, **53**, 976. doi: 10.1016/j.corsci.2010.11.030
23. M.P. Desimone, G. Grundmeier, G. Gordillo and S.N. Simison, *Electrochim. Acta*, 2011, **56**, 2990. doi: 10.1016/j.electacta.2011.01.009
24. R.A. Cherkasov and V.I. Galkin, *Russ. Chem. Rev*., 1998, **67**, no. 10, 857. doi: 10.1070/RC1998v067n10ABEH000421
25. M. Stern and A. L. Geary, *J. Electrochem. Soc*., 1957, **104**, no. 1, 56.
26. L. Zeng, G.A. Zhang, X.P. Guo and C.W. Chai, *Corros. Sci*., 2015, **90**, 202. doi: 10.1016/j.corsci.2014.10.011

27. G. Zhang, C. Chen, M. Lu, C. Chai and Y. Wu, *Mater. Chem. Phys*., 2007, **105**, 331. doi: 10.1016/j.matchemphys.2007.04.076
28. J.B. Sun, G.A. Zhang, W. Liu and M.X. Lu, *Corros. Sci*., 2012, **57**, 131. doi: 10.1016/j.corsci.2011.12.025
29. J.R. Macdonald, *J. Electroanal. Chem*., 1987, **223**, 25.
30. Y. Tan, Y. Fwu and K. Bhardwaj, *Corros. Sci*., 2001, **53**, 1254. doi: 10.1016/j.corsci.2010.12.015
31. F.M. Donahue and K. Nobe, *J. Electrochem. Soc*., 1965, **112**, 886.
32. M.P. Desimone, G. Gordillo and S.N. Simison, *Corros. Sci*., 2011, **53**, 4033. doi: 10.1016/j.corsci.2011.08.009
33. B.G. Ateya, B.E. El-Anadouli, F. M. El-Nizamy, *Corros. Sci*.,1984, 24(6), 509. doi: 10.1016/0010-938X(84)90033-7

♦ ♦ ♦